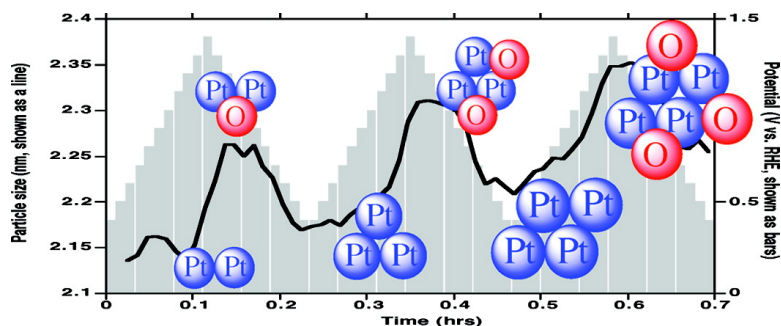Communication

In Situ Small-Angle X-ray Scattering Observation of Pt Catalyst Particle Growth During Potential Cycling

Matt C. Smith, James A. Gilbert, Jennifer R. Mawdsley, So#nke Seifert, and Deborah J. Myers

More About This Article

Additional resources and features associated with this article are available within the HTML version:

- Supporting Information
- Links to the 1 articles that cite this article, as of the time of this article download
- Access to high resolution figures
- Links to articles and content related to this article
- Copyright permission to reproduce figures and/or text from this article

View the Full Text HTML

In Situ Small-Angle X-ray Scattering Observation of Pt Catalyst Particle Growth During Potential Cycling

Matt C. Smith,*,† James A. Gilbert,† Jennifer R. Mawdsley,† Sönke Seifert,‡ and Deborah J. Myers†

Chemical Sciences and Engineering Division, and Advanced Photon Source, 9700 South Cass Avenue, Argonne, Illinois 60439

Received February 14, 2008; E-mail: mcqsmith@anl.gov

Polymer electrolyte fuel cells (PEFCs) promise a clean, efficient alternative to the internal combustion engine (ICE) via the electrochemical conversion of H_2 and O_2 to water and energy. Pt-containing electrocatalysts are used to facilitate the kinetics of the H_2 oxidation and O_2 reduction reactions.[1] However, the lifetime of PEFCs, and thus their commercial viability, is limited by degradation of the membrane–electrode assembly components.[2] This includes coarsening of the Pt electrocatalyst nanoparticles leading to the loss of electrochemically active surface area (ECA). This loss is exacerbated by particle size: the smaller the particle, the greater the thermodynamic force for its coarsening.[3,4] Thus, efforts to reduce the loading of expensive Pt by minimizing catalyst particle size (increasing ECA/weight Pt) are confounded by higher rates of ECA loss.[5] A better understanding of the mechanism of Pt degradation can provide the necessary information for the design of more durable catalysts and for definition of operating conditions that may alleviate or eliminate Pt particle growth.

To this end, we have used small-angle X-ray scattering (SAXS) to examine, in situ, a carbon-supported PEFC cathode electrocatalyst. An aqueous electrochemical cell with a non-adsorbing perchloric acid electrolyte was used as a model of the fuel cell cathode. SAXS is a well-established technique,[6] perfect for examining particle shape and sizes between 1 and 100 nm, appropriate for examination of state-of-the-art fuel cell electrocatalysts with particle sizes ranging from 2 to 4 nm. Additionally, SAXS is non-invasive and does not require the post-mortem approach of other imaging techniques, such as transmission electron microscopy (TEM), providing time-resolved analysis.

SAXS measurements were recorded at beamline 12-BM of the Advanced Photon Source at an energy of 11.5 keV using a MAR CCD detector. The Pt/C electrocatalyst (20 and 40 wt % Pt on XC-72 Vulcan carbon, E-Tek) was dispersed in perfluorosulfonic acid binder (5 wt % Nafion in aliphatic alcohol, Sigma-Aldrich) and supported on carbon sheet (Strem). The Pt/C electrode was immersed in 0.1 M $HClO_4$ electrolyte in a PTFE cell also containing a carbon counter electrode and a Ag/AgCl reference electrode. All potentials in this paper are referenced to the reversible hydrogen electrode. The Pt/C catalyst was potential cycled between 0.4 and 1.4 V at 10 mV s^{-1} with a 30 s potentiostatic hold every 50 mV. Background subtraction was performed by recording SAXS patterns of the cell minus the Pt electrocatalyst. This method has been shown to be valid for small-angle scattering.[7] To the authors' knowledge this is the first time that dynamic cycling of potentials has been reported in a SAXS experiment for Pt catalysts.

Our results for catalyst loadings of 0.4 mg cm^{-2} of 20 and 40 wt % Pt (**20-Pt** and **40-Pt**) are shown in Figure 1. Using IGOR software,[8] sizes were obtained from fitting as polydisperse spheres[9] between 0.1 < **Q** < 0.3 Å^{-1}, where **Q**, the scattering vector, the difference between the wave vectors of the incoming and the scattered radiation, is 4π

† Chemical Sciences and Engineering Division.
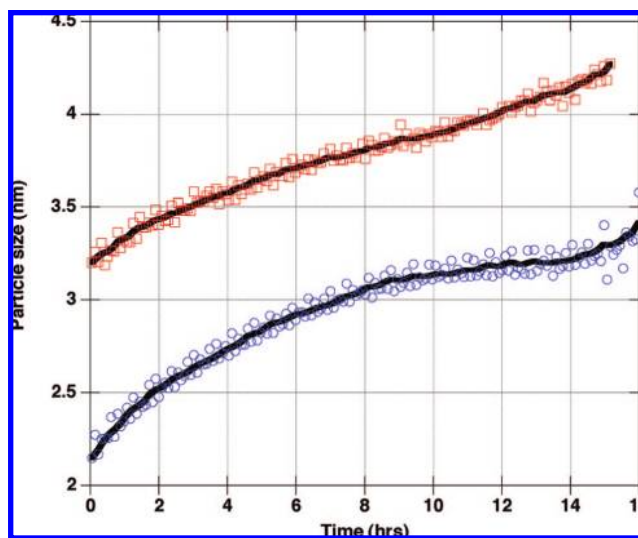‡ Advanced Photon Source.

Figure 1. SAXS data for 20 (○) and 40 (□) wt % Pt on XC-72 carbon, cycled between 0.4 and 1.4 V (vs RHE) in 0.1 M $HClO_4$. Fit lines (—) shown as a function of smoothing.

sin θ/λ, where θ is one-half of the scattering angle and λ is the photon wavelength. A single radius of gyration from a Guinier-type analysis[10] could not be determined as the samples did not contain a monodisperse particle size.

The particle size is seen to increase rapidly for **20-Pt** over the first 8 h before reaching slower growth at ~3.2 nm. Contrarily, **40-Pt**, whose particle size starts at 3.2 nm, exhibits a steady particle growth from the start. Pt particle growth with potential cycling of a PEFC cathode has recently been observed by Borup et al. using ex situ X-ray diffraction (XRD) and ECA loss measurements.[11] The particle growth we observe in the aqueous environment (2.1 to ~3.4 nm after 43 cycles between 0.4 to 1.4 V) is comparable to that observed by Borup et al. in the fuel cell environment (1.9 to ~4 nm after 300 cycles between 0.1 and 1.2 V; estimated from ECA loss and the ECA loss–particle size relationship).[11]

Figure 2 shows the fitting of the mean particle size and distribution to a Schulz function,[9,12] which has been used previously to successfully fit the distribution of Pt clusters supported on carbon.[13] Both **20-Pt** and **40-Pt** show clear progression of particle size with slight increase in distribution width. As shown, the final spectrum fits well to the postmortem TEM analysis. Similar good agreement has previously been observed for Pt_3Co particles using TEM, XRD, and a Gaussian fit of the SAXS[14] and for a TEM versus small-angle neutron scattering of Pt clusters.[7] Log-normal and Gaussian distributions showed poor agreement with the experimentally determined distributions, suggesting our data do not exclude long-range Pt ion transport (Ostwald ripening) as the ripening mechanism. Such a degradation mechanism should give a particle distribution substantially different than log-normal.[11]

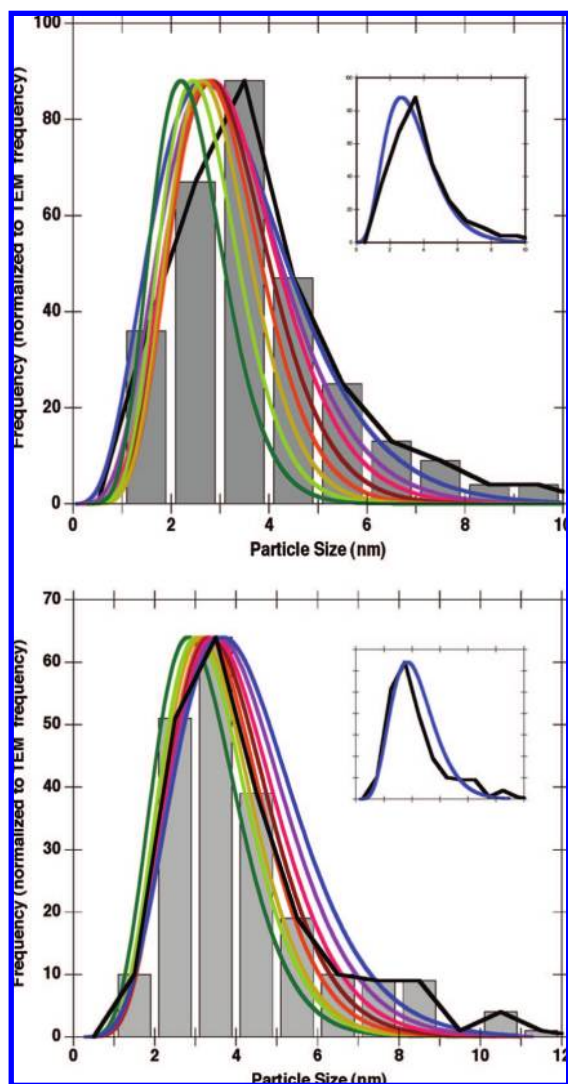**Figure 2.** **20-Pt** (top) and **40-Pt** (bottom) distribution calculated from TEM (black line, and histogram) and SAXS (start, green line, to finish, blue line), inset post-mortem distribution (black line) versus SAXS distribution at experiment end (blue line). Data for determination of distribution from SAXS were taken from data recorded at 0.4 V vs RHE.

Plotting particle size as a function of potential and potential cycle (Figure 3) shows overall particle growth with cycling with reversible and irreversible components to this growth. Potential-induced particle growth has been observed previously by Haubold et al. who noted a Pt particle size increase of 1 nm, which they attributed to oxide formation, when comparing samples held at 1.32 V to those held at 0.47 V.[15,16] We observe a particle growth of only ~0.1 nm between 0.4 and 1.4 V, as shown in Figure 3 for the **20-Pt** sample, the majority of which is reversible with return of the potential to 0.4 V. Due to the reversibility of this particle growth with potential and the correspondence between this growth and the oxidation−reduction currents observed at these potentials, we attribute this growth to oxide formation. The ionic radii of the O^{2-} ion is 1.40 Å,[17] thus the observed growth of 0.1 nm would suggested an incomplete monolayer of oxygen, assuming a spherical Pt particle. However, over the duration of the 16 h potential cycling experiment, the overall Pt particle growth at 0.4 V, a potential at which Pt is oxide-free,[18] was observed to be 1 nm, similar to the growth observed by Haubold et al.

Figure 3 displays several interesting features: (1) the general trend of Pt particle size increase can be observed over relatively few scans and (2) the size maxima occur after the voltage potential maxima. Two
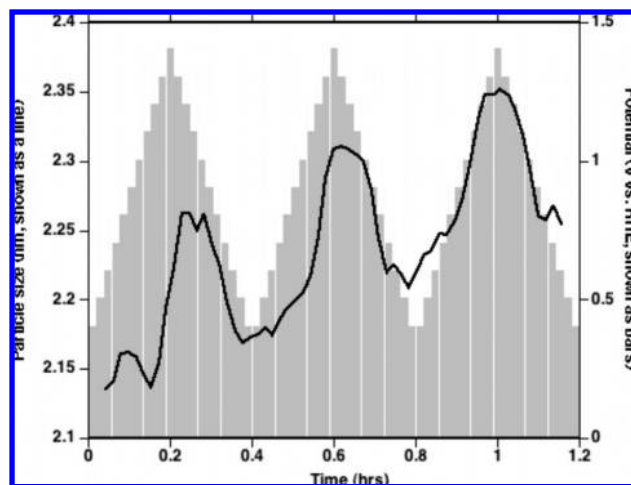

Figure 3. **20-Pt** catalyst size observed over initial three potential cycles.

possible causes of this latter feature are further formation of the oxide layer during the cathodic potential scan, indicating that an equilibrium oxide coverage was not established during the 30 s potentiostatic hold at 1.4 V, or deposition of solution phase Pt formed at 1.4 V onto the Pt particle during the potential hold at 1.3 V. As discussed earlier, the latter process, Pt dissolution and re-deposition (Ostwald ripening), is a potential mechanism for potential cycling-induced particle growth. To the authors' knowledge this is the first in situ observation of platinum nanoparticle growth during potential cycling through the oxide formation−reduction potential region.

Supporting Information Available: Complete ref 2. This material is available free of charge via the Internet at http://pubs.acs.org.

References

(1) Gasteiger, H. A.; Kocha, S. S.; Sompalli, B.; Wagner, F. T. *Appl. Catal. B* **2005**, *56*, 9–35.
(2) Borup, R.; et al. *Chem. Rev.* **2007**, *107*, 3904–3951.
(3) Darling, R. M.; Meyers, J. P. *J. Electrochem. Soc.* **2005**, *152*, A242–A247.
(4) Darling, R. M.; Meyers, J. P. *J. Electrochem. Soc.* **2003**, *150*, A1523–A1527.
(5) Makharia, R.; Kocha, S. S.; Yu, P. T.; Sweikart, M. A.; Gu, W.; Wagner, F. T.; Gasteiger, H. A. *ECS Trans.* **2006**, *1*, 3–18.
(6) Narayanan, T. *Soft Matter: Scattering, Imaging and Manipulation*, 1st ed.; Borsali, R., Pecora, R., Eds.; Springer: Berlin, 2007.
(7) Coppola, R.; Giorgi, L.; Lapp, A.; Magnani, M. *Physica B* **2000**, *276*, 839–840.
(8) *IGOR Pro 6*, http://www.wavemetrics.com/.
(9) Kotlarchyk, M.; Chen, S. H. *J. Chem. Phys.* **1983**, *79*, 2461–2469.
(10) Guinier, A.; Fournet, G. *Small-Angle Scattering of X-Rays*; John Wiley & Sons: New York, 1955.
(11) Borup, R. L.; Davey, J. R.; Garzon, F. H.; Wood, D. L.; Inbody, M. A. *J. Power Sources* **2006**, *163*, 76–81.
(12) Aragon, S. R.; Pecora, R. *J. Chem. Phys.* **1976**, *64*, 2395–2404.
(13) Tsao, C. S.; Chen, C. Y. *Physica B* **2004**, *353*, 217–222.
(14) Borchert, H.; Shevehenko, E. V.; Robert, A.; Mekis, I.; Kornowski, A.; Grubel, G.; Weller, H. *Langmuir* **2005**, *21*, 1931–1936.
(15) Haubold, H. G.; Wang, X. H.; Goerigk, G.; Schilling, W. *J. Appl. Crystallogr.* **1997**, *30*, 653–658.
(16) Haubold, H. G.; Wang, X. H.; Jungbluth, H.; Goerigk, G.; Schilling, W. *J. Mol. Struct.* **1996**, *383*, 283–289.
(17) *CRC Handbook of Chemistry and Physics*, 73rd ed.; CRC Press: Boca Raton, FL, 1992.
(18) Teliska, A.; O'Grady, W. E.; Ramaker, D. E. *J. Phys. Chem. B* **2005**, *109*, 8076–8084, and references therein.

JA801138T